Spectroscopic Study and Simulation from Recent Structural Models for Eumelanin: I. Monomer, Dimers

Klaus B. Stark*

Accelrys Inc., 9685 Scranton Road, San Diego, California 92121-3752

James M. Gallas

Department of Physics and Astronomy, University of Texas at San Antonio, San Antonio, Texas 78249

Gerry W. Zajac

BP Research Center, P.O. Box 3011, Naperville, Illinois 60566-7011

Melvin Eisner

Department of Physics, University of Houston, Houston, Texas 77004

Joseph T. Golab

BP Research Center, P.O. Box 3011, Naperville, Illinois 60566-7011

Received: July 31, 2002; In Final Form: January 9, 2003

Spectroscopic simulations of a leading structural model for melanin, the pigment responsible for coloration and photoprotection in humans and animals, were done. We performed density functional theory (DFT) calculations using both the local density approximation (LDA) and the generalized gradient approximation (GGA) on a recent structural model for eumelanin based on higher oligomers of the monomer of neutral 5,6-indolequinone and its reduced forms, semiquinone and hydroquinone. This paper reports on our semiempirical spectroscopic simulations for the monomer and dimer energy-minimized structures. Our second study (part II) extends this approach to higher oligomers (tetramers through hexamers) and points out that the known optical spectra of eumelanins can be adequately explained on this basis.

1. Introduction

The melanins are a widely occurring class of biological pigments that provide coloration and photoprotection to animals and plants and have been the subject of extensive studies.[1−6] The melanins describe a series of pigments that are classified into roughly three classes: eumelanins, black and dark-brown nitrogen-containing pigments; phaeomelanin pigments, which contain sulfur and give rise to coloration such as red hair; and plant phila pigments termed allomelanins.

The eumelanins are also universally considered to be photoprotective, as evidenced by an optical absorption spectrum that increases monotonically with energy of the light and matches the action spectrum for tissue damage. We will restrict this discussion to the eumelanins, which are involved in human pigmentation.

An understanding of the molecular basis for the optical absorption of eumelanin is both intriguing and challenging. How does optical absorption follow from the structure of a polymer that has tuned itself to the absorption of sunlight, in an evolutionary process that spans many millions of years, with the apparent intent of photoprotection? Unfortunately, an adequate explanation of the eumelanin absorption spectrum has not been available, largely because the eumelanin structure has been essentially unknown and much debated.

Recently, however, a new representation for a structural model was proposed that is based on aggregation of oligomeric units that promises to adequately describe the optical absorption spectrum of eumelanins.[7−14] Although there is little understanding of melanin morphology, structure, and even size, there has been some agreement regarding the molecular units that comprise the polymerized structure. Typical units include dihydroxyindole (HQ), dihydroxyindole carboxylic acid (DHICA) and 5,6-indolequinone (IQ). Molecular orbital calculations were first performed by Pulman and Pulman (*Biochim. Biophys. Acta* **1961**, *54*, 384) on monomers of 5,6-indolequinone where some important molecular properties for melanin were predicted that were in accord with experimental data known for the polymer. In particular, the strong electron-donor and -acceptor qualities of the units were predicted.

Previously, a series of pioneering and careful ab initio and semiempirical calculations were performed[15] on IQ monomers and the reduced forms, semiquinone (SQ) and hydroquinone (HQ), and their charge states. These calculations revealed that IQ, SQ, and HQ are all good electron acceptors, which could be a basis for an efficient cellular protection mechanism against damage by free radicals. Although some connections with the optical absorption spectra of eumelanins were referenced by the inclusion of higher anionic states (−1, −2), these calculations[15] were based on monomeric units. We believe that any successful explanation of the melanin absorption spectrum should be based

* Corresponding author. E-mail: kstark@accelrys.com.

10.1021/jp0266594 CCC: $25.00
Published on Web 03/12/2003

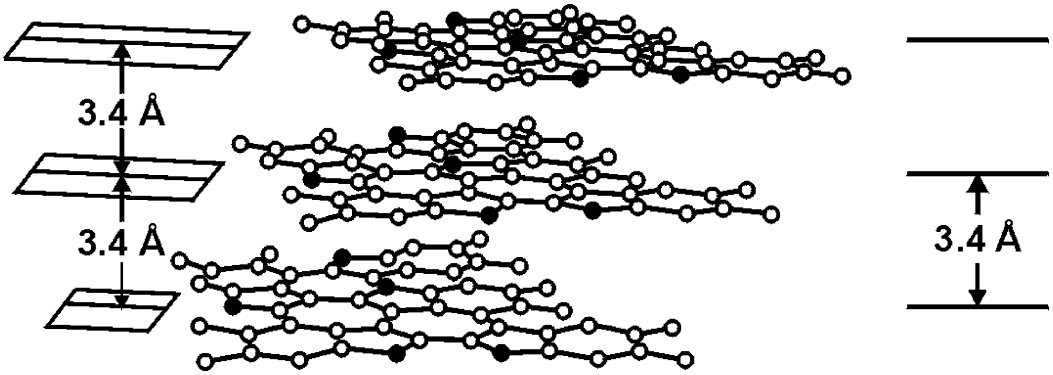

Figure 1. Schematic representation of a melanin protomolecule. Five to seven monomers of 5,6-indolequinone are arranged in a plane, forming three to four layers stacked 3.4 Å apart. The white circles in the framework represent carbon atoms, and the dark circles represent nitrogen atoms. The quinone oxygen atoms are also represented as white cirlces, and the hydrogen atoms are not represented. (Figure taken with kind permission from ref 8.)

on structural models that incorporate oligomers and also incorporate experimental data relating to melanin size and morphology.

Previous small-angle X-ray studies on solutions of melanin derived from various sources reported nanometer-sized particles but made no reference to any structural details for this particles.[16] More recently, wide-angle X-ray scattering[7,8] and scanning tunneling microscopy (STM),[9−11] atomic force microscopy,[12] and small-angle X-ray scattering (SAXS)[13] studies have revealed nanometer-sized particles that were described in terms of smaller fundamental units, and aggregates thereof, that constituted eumelanins in aqueous media.

These results have led to the proposal of a nanometer-sized protomolecule model structure for eumelanin consisting of the covalently bonded monomers of 5,6-indolequinone to form single sheets with lateral extents of 15−20 Å that are stacked with ∼3.4-Å spacings to a nanometer extent—that is, the model proposed earlier by Chio[5] as a local melanin structure. Melanins are then considered to be an aggregation of these fundamental units.[9,13]

A typical molecular model of such a protomolecule is shown in Figure 1. This model for the melanin protomolecule is simplified in several respects. First, it is a homopolymer representation—using 5,6-indole quinone (IQ), and its reduced form dihydroxy indole (HQ), as the basic structural units—whereas the various quinone and phenolic intermediates that occur from the redox polymerization and are believed to form the actual melanin heteropolymer are not represented here for simplicity. We believe that such a simplification will not affect our aims and goals of the present paper: to describe the optical absorption of melanin.

Additional support for this molecular model for eumelanin has been demonstrated for natural sepia eumelanin by atomic force microscopy, which revealed multi-nanometer-sized filaments and spherical aggregates of which smaller constituents were detected.[12] Some of these studies[9−13] also suggested that synthetic and natural melanins are also aggregates of the protomolecules. In light of these recent morphological studies, it is appropriate to extend the pioneering computational studies[17−19] to include the proposed eumelanin structures based on the recent morphological characterizations of both synthetic and natural eumelanins at the mesoscopic scale.

The goal of this study is to generate, from these eumelanin molecular models, energy-minimized structures that provide the electronic structure and subsequent optical absorption spectra from semiempirical calculations. Although the techniques are understood to be approximate, agreement with experimental results should offer additional support to the molecular model and also provide new predictions on which to base further experimentation and understanding of melanin structure. The work might also lead to further refinement of the structural model.

2. Calculational Details

All structure optimizations were performed using Accelrys's density functional theory (DFT) program DMol^3.[20] DMol^3 utilizes a basis set of numeric atomic functions that are exact solutions to the Kohn−Sham equations for the atoms.[21] These basis sets are generally more complete than a comparable set of linearly independent Gaussian functions and have been demonstrated to have small basis set superposition errors.[21] In the present study, a polarized split valence basis set, termed a double-numeric-polarized (DNP) basis set, was used. The calculations were performed using both the local VWN[22] functional and the nonlocal BP[23] functional.

Atom-centered grids were used for the numerical integration. The particular grid used about 1000 grid points for each atom in the calculation and corresponds to the "Medium" option in DMol.[24] A real space cutoff of 4 Å was used for the numerical integration.

All SCF calculations were converged to a root-mean-square (rms) change in the charge density of less than 1×10^{-5} Ha. Geometries were optimized using analytic gradients and an efficient algorithm employing delocalized internal coordinates.[25] Geometries were optimized so that the change of energy was less than 2×10^{-5} Ha and the change of the maximum force on the atoms was less than 0.004 Ha/Å.

For the DFT-optimized structures, absorption spectra were calculated using the Pair excitation configuration interaction (PECI) method[26] and the AM1 Hamiltonian[27] as implemented in the semiempirical program VAMP[28] available from Accelrys Inc. In the PECI method, excited states are calculated by including all single and all double excitations in which a complete electron pair is promoted. This is a very economical and effective CI expansion for closed-shell molecules and is used in VAMP for the calculation of spectra or hyperpolarizabilities. In the current calculation, eight orbitals were included in the PECI expansion.

3. Results

Monomers. The motiviation for this work stems from the fact that there is evidence that planar oligomers of 5,6-indolequinone (IQ) monomers and/or the reduced forms, semi-

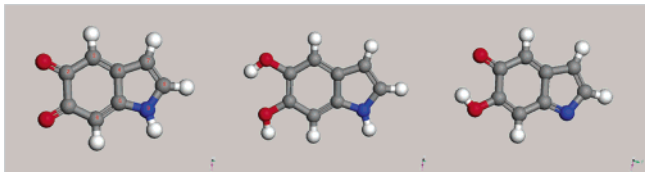

Figure 2. From left to right: structures of 5,6-indolquinone (IQ), hydroquinone (HQ), and semiquinone (SQ). Carbon atoms are displayed in gray, oxygen atoms in red, nitrogen atoms in blue, and hydrogen atoms in white.

TABLE 1: Calculated Bond Distances (in Angstroms) and Angles (in Degrees) of the IQ Monomer

bond	BGC[a]	VWN	BP	angle	BGC[a]	VWN	BP
C1−C2	1.56	1.56	1.58	C3−C2−C1	118.2	118.6	118.3
C3−C2	1.48	1.44	1.46	C4−C3−C2	119.4	119.4	119.8
C4−C3	1.33	1.36	1.37	C5−C4−C3	121.7	120.9	120.9
C5−C4	1.49	1.47	1.48	C6−C5−C4	124.4	124.5	124.6
C6−C5	1.33	1.35	1.36	C7−C4−C3	132.8	132.7	132.7
C7−C4	1.46	1.44	1.46	C8−C7−C4	107.1	107.2	107.3
C8−C7	1.33	1.36	1.37	N9−C5−C4	105.6	106.0	105.9
N9−C5	1.37	1.37	1.39	O10−C1−C2	118.8	118.6	119.1
O10−C1	1.19	1.22	1.23	O11−C2−C1	119.2	118.4	119.2
O11−C2	1.18	1.22	1.23				

[a] BGC values from ref 15.

TABLE 2: Calculated Bond Distances (in Angstroms) and Angles (in Degrees) of the HQ Monomer

bond	BGC[a]	VWN	BP	angle	BGC[a]	VWN	BP
C1−C2	1.42	1.41	1.42	C3−C2−C1	120.4	120.6	120.5
C3−C2	1.37	1.38	1.39	C4−C3−C2	119.9	119.0	119.2
C4−C3	1.40	1.40	1.41	C5−C4−C3	118.9	119.3	119.1
C5−C4	1.39	1.41	1.42	C6−C5−C4	121.8	122.2	122.2
C6−C5	1.40	1.39	1.40	C7−C4−C3	134.3	133.9	134.0
C7−C4	1.44	1.42	1.44	C8−C7−C4	106.7	107.2	107.2
C8−C7	1.35	1.37	1.38	N9−C5−C4	107.8	107.3	107.3
N9−C5	1.37	1.37	1.39	O10−C1−C2	116.4	113.4	114.5
O10−C1	1.35	1.37	1.38	O11−C2−C1	116.2	118.2	119.7
O11−C2	1.36	1.35	1.39				

[a] BGC values from ref 15.

quinone (SQ) and hydroquinone monomers, form the structural subunits of the complex melanin biopolymer studies.[1−6]

Therefore, it is important to first examine these monomers and calculate their UV/vis spectra so that comparisons with existing literature data can be made. The three molecules are displayed in Figure 2. A recent paper[15] by L. E. Bolivar Martinez et al. (henceforth referred to as BGC) dealt with geometric and spectroscopic studies of these monomers. The current calculations in this first study, part I, should mainly help to calibrate the modeling strategy for the oligomers, which are to be considered later, in part II (to be published). The three structures of Figure 2 have been energy-optimized using Accelrys's density functional theory (DFT) program DMol[3] [20] using both the local density approximation (LDA) with the VWN[22] functional and the generalized gradient approximation (GGA) with the BP[23] functional. The results are summarized in Tables 1−3, where they are compared with ab initio results obtained by BGC.[15] The atom numbering of Tables 1−3 is shown in Figure 3 in the case of IQ.

A close inspection of Tables 1−3 shows that the DFT results of this study nicely agree with the ab initio results of BGC. The only noteworthy discrepancy arises for certain O−C−C angles and some C−O bond distances. Even here, the largest differences are about 4−5%. It also shows the efficiency of the numerical basis sets employed in DMol[3], which provide an

TABLE 3: Calculated Bond Distances (in Angstroms) and Angles (in Degrees) of the SQ Monomer

bond (Å)	BGC[a]	VWN	BP	angle (deg)	BGC[a]	VWN	BP
C1−C2	1.52	1.49	1.51	C3−C2−C1	117.9	120.4	119.5
C3−C2	1.49	1.45	1.48	C4−C3−C2	119.6	117.5	118.2
C4−C3	1.32	1.34	1.36	C5−C4−C3	121.2	121.1	121.0
C5−C4	1.49	1.49	1.50	C6−C5−C4	121.7	122.1	121.6
C6−C1	1.33	1.35	1.36	C7−C4−C3	135.7	134.4	134.7
C7−C4	1.45	1.44	1.46	C8−C7−C4	105.0	104.9	105.0
C8−C7	1.33	1.35	1.36	N9−C5−C4	112.1	110.9	111.4
N9−C5	1.27	1.30	1.31	O10−C1−C2	112.3	112.3	114.1
O10−C1	1.33	1.32	1.35	O11−C2−C1	120.6	116.3	117.7
O11−C2	1.18	1.23	1.24				

[a] BGC values from ref 15.

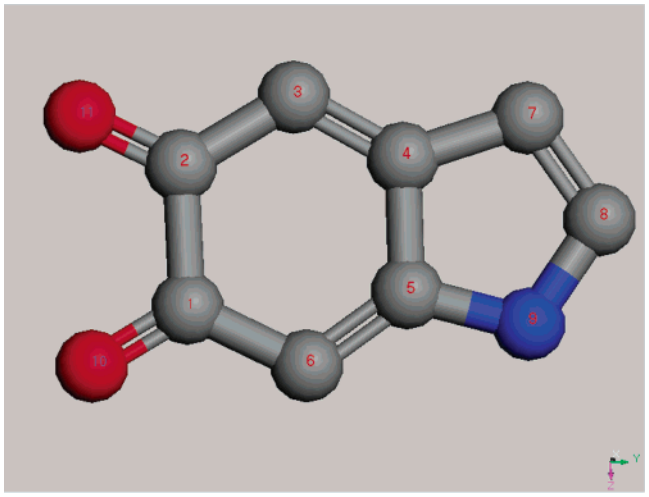

Figure 3. Atom numbering in Tables 1−3 exemplified for the IQ monomer (without hydrogens).

accuracy that can be achieved only by much larger basis sets when the traditional Gaussian basis set scheme is used.[20]

More important for this study is that the results obtained in the local density approximation are almost identical with those obtained using the computionally more expensive generalized gradient approximation scheme. This reflects the well-known fact that, for structure optimization, the LDA scheme is often sufficient[29−31] and that GGA calculations, which are roughly twice as expensive as LDA calculations, do not always need to be performed if one is only interested in obtaining good molecular geometries.[32−34]

In their 1999 paper, BGC claim that semiempirical Hamiltonians, such as the PM3 Hamiltonian,[35] give—at a fractional computational cost—optimized structures for the monomers that are very close to the ab initio optimized geometries.[15] However, the monomer structures of BGC showed slight deviations from planarity when the optimizations were performed using the PM3 Hamiltonian. This effect is expected to be more pronounced for the higher oligomers, as exemplified by a sample geometry optimization for a possible tetramer structure, the results of which are displayed in Figure 4.

The DFT-optimized structure in Figure 4a is almost planar, whereas the structure resulting from a geometry optimization using VAMP and the PM3 Hamiltonian (Figure 4b) shows significant deviations from planarity. In particular, the oxygen atoms of the carbonyl groups are dragged above and underneath the plane formed by the indolequinone rings. Indeed, a DFT−GGA single-point energy calculation on the structure of Figure 4b showed that it is more than 30 kcal/mol less stable than the structure displayed in Figure 4a. Moreover, deviations from

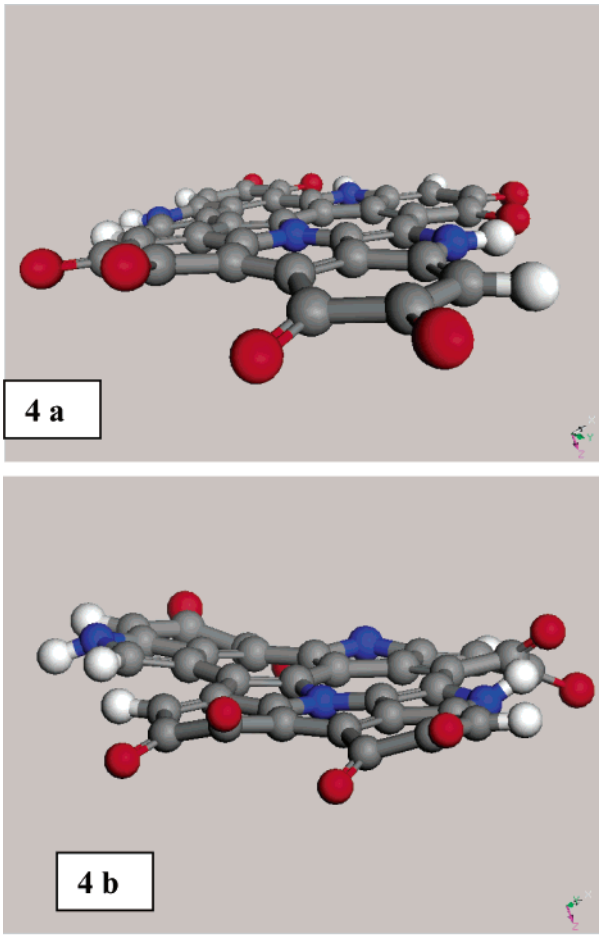

Figure 4. Tetramer structure optimized with (a) DFT−LDA and (b) PM3. Atom coloring as in Figure 2.

TABLE 4: Computed λ_{max} Values (in Nanometers) for the Three Monomers of Figure 2

molecule	BGC[a]	PECI
IQ	243	243
HQ	202	201
SQ	248	224

[a] BGC values from ref 15.

planarity affect the extent of conjugation in the oligomers, which, in turn, would lead to different UV/vis spectra.

Because the higher oligomers will be explicitly treated in a later study, all geometry optimizations were carried out on the DFT−LDA level of theory, even for the monomers and dimers, to guarantee consistency. For the structures of Figure 2, UV/vis spectra were calculated using the pair excitation configuration interaction (PECI)[26] method and the AM1 Hamiltonian[27] as implemented in the semiempirical program VAMP.[28] λ_{max} (wavelength at maximum absorption) values for the IQ, HQ, and SQ monomers are listed in Table 4, where they are also compared to the values obtained by BGC. In the BGC paper, ZINDO−CI calculations[36] were carried out on the geometry obtained with the PM3 Hamiltonian. BGC showed that the structures obtained within the semiempirical approximation were very similar to their ab initio geometries, and they therefore chose an all-semiempirical approach to obtain the electronic spectra. However, as discussed above, the PM3 geometries showed slight deviations from planarity, which might influence the results for the spectra calculations (see discussion below).

The ZINDO−CI method used by BGC has been successfully applied for optical spectra calculations in numerous applications

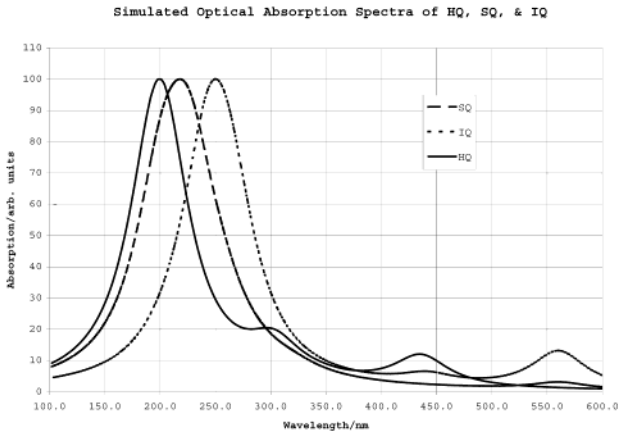

Figure 5. Simulated optical absorption spectra of HQ, SQ, and IQ.

(see, e.g., ref 37). The PECI method for obtaining excited states applied in this paper also has a track record of successful applications.[26,38,39] Both methods of obtaining electronic spectra should produce results of comparable quality. In their paper, BGC did not mention, however, whether they included double excitation in their CI expansion of used only single excitations. Therefore, a more detailed comparison between the PECI results obtained in this paper and the ZINDO−CI results of BGC is difficult.

The agreement between the VAMP results and those obtained by BGC for IQ and HQ is excellent (Table 4). The BGC and VAMP results for SQ differ by 24 nm. However, it must be noted that the structural differences for this monomer when compared to the structure obtained by BGC were larger than those for IQ and HQ monomer (see Tables 1−3). This might be the cause for the slight deviation in the absorption maximum. It also has to be mentioned that BGC used the PM3 Hamiltonian, whereas the present study uses the AM1 Hamiltonian. The differences between the PM3 and AM1 results, however, were found to be small in the present study. The agreement of the PECI-AM1 spectra with the spectra obtained by BGC, who used a different CI scheme, was somewhat better than for the spectra resulting from PECI−PM3. Therefore, the AM1 Hamiltonian was used for all spectra calculations. The spectra for all three monomers as obtained by VAMP−PECI are displayed in Figure 5. The absorption spectrum for IQ (dotted line in Figure 5) obtained by VAMP is in excellent agreement with the earlier spectrum of BGC. Two maxima are obtained, one at 243 nm (BGC, 243 nm) and a smaller absorption at larger wavelengths, again in agreement with the BGC results. The simulated HQ absorption spectrum (solid line in Figure 5) shows a maximum absorption peak at 201 nm, which also appeared in the BGC spectrum (202 nm). The spectrum shows additional absorptions around 300 and 440 nm that are not visible in the spectra of BGC. The additional peak at 440 nm is small, however. Optical data available for HQ, shown in Figure 6, suggest partial agreement with the simulated data for HQ. The experimental spectrum for HQ also shows a peak at 270 nm that is not predicted by our calculations. Given the very high reactivity of the melanin precursors, it is possible that any residual oxygen will cause subsequent polymerization in the samples of HQ used to prepare any experimental spectra. If this did occur, it could produce absorption peaks in the region of 270 nm. If the experimental peak is not an artifact, then it indicates that our calculations, and/or the structures chosen for the calculations, simply do not predict this peak.

The optical spectrum of SQ as obtained by VAMP (dashed line in Figure 5) is qualitatively very similar to the spectrum

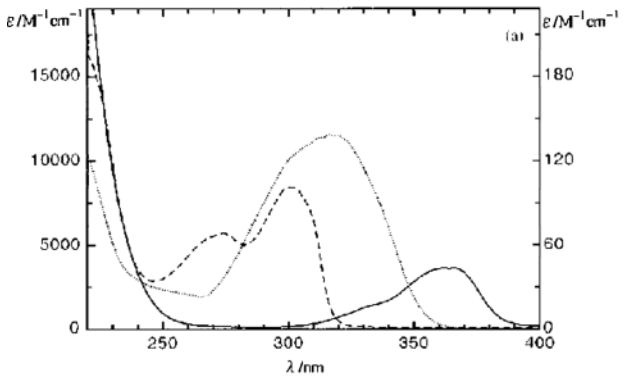

Figure 6. Experimental optical absorption spectrum of HQ in acetonitrile *[*taken with kind permission from Zhang, X.; Erb, C.; Flammer, J.; Nau, W. M. *Photochem. Photobiol.* **2000**, *71* (5), 524]. The HQ spectrum (dashed lines) shows bands at 300, 270, and just below 200 nm.

obtained by BGC. It is dominated by a large absorption at low wavelengths and shows a late and very weak absorption around 500 nm. The absorption maximum is shifted to somewhat lower wavelengths (224 nm as compared to 248 nm in BGC) in the present study, however. A VAMP−PECI calculation on the PM3 geometry for SQ obtained by BGC shifted the λ_{max} value slightly to 230 nm. Therefore, the discrepancy for the λ_{max} value must be mainly attributed to the different excitation scheme used by BGC to obtain the optical spectrum.

It is important to note that the simulation data obtained by VAMP−PECI provide only the oscillator strengths at a point, which makes it difficult to make comparisons with experimental data because the broadening of the spectral lines more familiar to the spectroscopist are missing. The solvent interactions and orientations are partly responsible for the inhomogeneous broadening effects in optical spectra. Because of the coupling to the environment around the molecule, a finite lifetime for the excited states is expected, which is empirically modeled by a Lorentzian broadening of the theoretical spectra in this work.

Whereas the implementation of band broadening into the simulated data is not arbitrary, the full width at half-maximum (fwhm) would be arbitrary. In this regard, we chose to implement band-broadening of the data with a somewhat arbitrary Lorentzian broadening of 40 nm that is at least in accord with experimental data, as shown by the experimentally derived optical absorption spectrum of Figure 6 for HQ in acetonitrile.

A remaining issue is further solvent-induced broadening of the electronic spectra because of the increased conjugation associated with the larger dimers. These effects are ignored in the present treatment.

Dimers. Five possible dimer structures have been optimized using DMol[3] on the LDA/VWN and GGA/BP levels of theory. The optimized structures of dimers I−V are displayed in Figure 7a−e. The energies of the five dimers at 0 K relative to the most stable dimer are listed in Table 5. Both LDA and GGA functionals predict the entirely planar dimer 3 (Figure 7c) to be the most stable structure. This is due to a hydrogen bond that forms between the hydrogen at the indole nitrogen and the adjacent carbonyl oxygen atom. However, the LDA functional stabilizes dimer 3 relatively more than the GGA functional: whereas the difference to the next stablest dimer is about 8 kcal/mol using the VWN functional, it is only 5 kcal/mol using the BP functional. This is due to the well-known tendency of LDA to overbind.[30a,b] Indeed, the hydrogen bond formed is predicted to be 1.68 Å long, whereas it turns out to be 1.80 Å with the

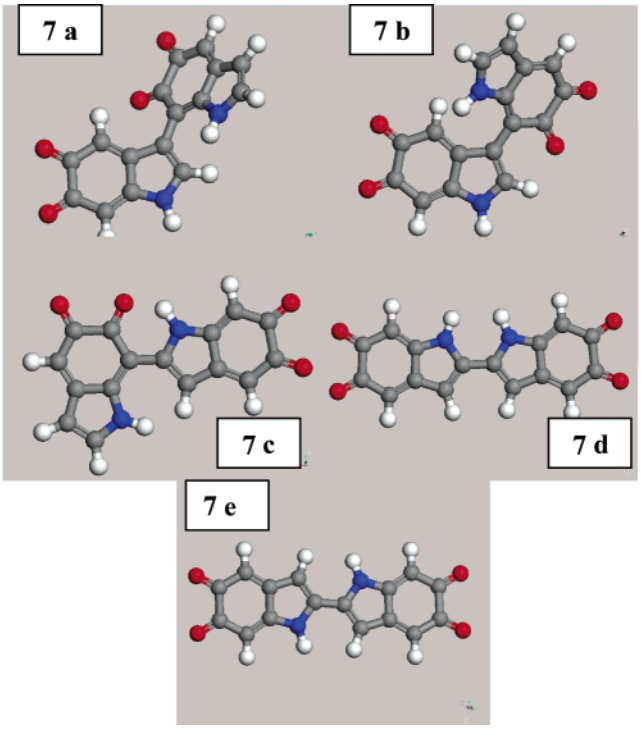

Figure 7. LDA-optimized dimer structures: (a) dimer 1, (b) dimer 2, (c) dimer 3, (d) dimer 4, (e) dimer 5. Atom coloring as in Figure 2.

TABLE 5: Relative Energies (in kcal/mol) of Dimer Structures at 0 K

structure	VWN	BP
dimer 1	14.6	11.3
dimer 2	7.8	6.7
dimer 3	0.0	0.0
dimer 4	10.5	4.9
dimer 5	13.5	7.7

BP functional. The latter value is certainly more realistic. Apart from this structural feature, the LDA and the GGA structures are very similar. Dimer 1 (Figure 7a) is predicted to be the least stable of the five structures under consideration by both levels of theory. Both monomer units are significantly twisted out of the planar conformation (by about 50° in the GGA approximation). Although hydrogen bonding would be possible in a planar conformation, the hydrogen atoms of the five-membered rings would be to close to each other, leading to a repulsion that outweighs the gain in energy by the former interaction.

The GGA calculation predict dimer 4 (Figure 7d) to be the second most stable structure, followed by dimer 2 (which is a rotamer of dimer 1) and dimer 5 (which is a rotamer of dimer 4) (see Figure 7b and e, respectively). The energy difference between dimer 4 and dimer 3 is predicted to be about 5 kcal/mol by the GGA calculations. This reflects the lack of a hydrogen-bond interaction, which is missing in dimer 4. Dimer 4 is not completely planar, as the monomer units are twisted against each other by about 9.5°. This is due to H−H repulsion in a completely planar dimer. Dimers 2 and 5 are predicted to be of very similar stability by the GGA calculations, the energy difference between them being only 1 kcal/mol. This energy difference is actually less than the accuracy that can be delivered by current density functionals,[30b] so that definitive statements about their relative stabilties cannot be made using this level of theory. The VWN calculations give a different stability ranking for dimers 2, 4, and 5. However, it is well-known[40] that, within the LDA approximation, relative energies and transition state energies are often not reliable, although the

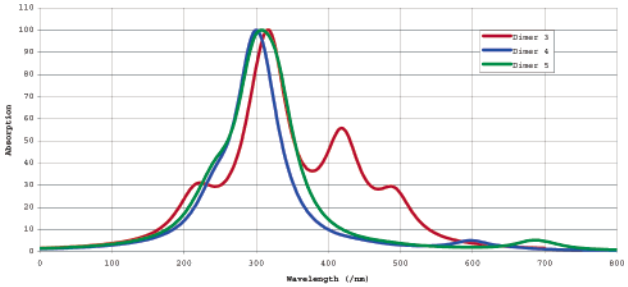

Figure 8. Simulated absorption spectra of dimers 3−55.

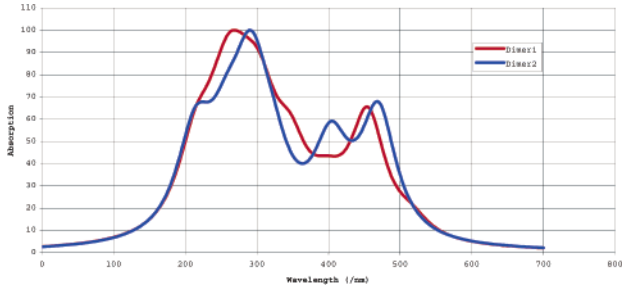

Figure 9. Simulated absorption spectra of dimers 1 and 2.

TABLE 6: HOMO-LUMO Gaps, Torsions, and Maximum Absorption Wavelengths for Dimers 1−5

dimer	HOMO−LUMO gap[a]	ϕ_{dimer}[b] (deg)	λ_{max} (nm)
1	20.9	127.9	261
2	18.2	39.2	289
3	14.7	0.6	319
4	17.0	9.5	295
5	16.2	0.5	294

[a] In kcal/mol, calculated on the BP/DNP level. [b] Torsional angle across the dimer bond.

overall structures are very similar to those obtained with gradient corrections. Therefore, an analysis of relative stability based on total energy calculations is performed only for the results obtained with the BP functional.

The absorption spectra of dimers 3−5 are shown in Figure 8. The most stable dimer, dimer 3, shows a significant bathochromic shift of about 80 nm compared to the monomers, exhibiting an absorption maximum at 320 nm. This is expected as the planar structure of this dimer contributes to a stronger delocalization and thereby induces a red shift in the absorption spectrum. The red shifts of dimers 4 and 5 are somewhat lower, with maxima around 300 nm. This is due to the already mentioned slight deviations from planarity.

The calculated absorption spectra of dimers 1 and 2 are shown in Figure 9. Figure 9 shows that, for dimers 1 and 2, the strong absorptions characterizing the monomer spectra and the dimer spectra in Figure 8 have largely vanished. The spectra of dimers 1 and 2 show only broad absorptions with low intensities. This is due to the largely nonplanar geometries of these compounds, as shown in Figure 7a and b.

The shift in the absorption maxima is accompanied by a low-energy shift in the band gaps. This is illustrated in Table 6, which summarized the energy gaps between the highest occupied molecular orbital (HOMO) and the lowest unoccupied molecular orbital (LUMO) as calculated at the BP/DNP level, together with a structural parameter ϕ_{dimer}, the torsional angle across the dimer bond. The λ_{max} values for the different dimers are also included in Table 6.

Although the absolute values of HOMO−LUMO gaps predicted at the DFT level are not reliable,[41] the values in Table 6 clearly show the trend that the most delocalized and stable system (dimer 3, $\phi_{dimer} = 0.6°$), which exhibits the largest red shift ($\lambda_{max} = 319$ nm) in the optical spectrum, also has the lowest HOMO−LUMO gap (14.7 kcal/mol). The nonplanar dimers 1 and 2 ($\phi_{dimer} = 127.9°$ and 39.2°, respectively), on the other hand, show the largest gaps (20.9 and 18.2 kcal/mol, respectively) and lowest red shifts ($\lambda_{max} = 261$ and 289 nm, respectively), whereas the almost-planar structures 4 and 5 have intermediate values. Therefore, the shift in the absorption maxima can be correlated to a shift in an electronic property (HOMO−LUMO gap), as well as to a change in a structural parameter (rotation around the dimer bond). In general, the lower the HOMO−LUMO gap, the larger the red shift, and the larger the deviation from planarity, the larger the HOMO−LUMO gap and, therefore, the lower the red shift.

4. Conclusions

The goal of the present work is to explore the structure−function relationship for a recently proposed structure for eumelanins by simulating their physical and chemical properties employing QM simulation techniques. This work utilizes a molecular orbital treatment of the monomers and dimers believed to comprise the melanin polymer as a comparison between the two different techniques used for the energy minimization process and also as a starting point for the extension to larger oligomers (tetramers, pentamers, etc.) that correspond to the new model.

Of particular interest for the comparison is the predicted structural geometries (bond lengths, angles, and final morphologies) and also the electronic transitions, especially the HOMO and the LUMO energies. The predicted electronic transitions allow us to make the final important comparison of the experimental absorption spectra for melanin and its subunits.

Monomers. On the matter of comparison of energy-minimization techniques used to obtain the simulated monomer structure, the results for the DFT method agree very well with those obtained by BGC for the three monomeric melanin subunits, as seen in Tables 1−3 where bond distances and angles agree generally within a few percent.

A more interesting difference detailed by the two techniques concerns the slight deviation from planarity for the monomer structures simulated by the BGC approach using the PM3 Hamiltonian. As expected, this feature became still more pronounced for the larger oligomers, as illustrated if Figure 4 for the case of the tetramer. Whereas the DFT-optimized structure remains almost planar, that optimized using VAMP and the PM3 Hamiltonian differs significantly from planarity. This is an important issue because the deviation from planarity affects the extent of conjugation, which, in turn, should be reflected in the optical absorption spectra for the full melanin structure.

With regard to the calculation of the optical spectra, electronic transitions were obtained by the PECI method in VAMP applied to the DFT-optimized structures. The λ_{max} values for the IQ, HQ, and SQ monomers, listed in Table 4, compare quite well with those obtained by BGC, except for the case of the semiquinone monomer, which is expected because there are greater structural differences between the two methods for this monomer. Also, the different excitation scheme used by BGC contributes to this discrepancy.

To present the data in a manner more meaningful and familiar to the biochemist or biologist, we chose to broaden the electronic spectra in a partially arbitrary manner that incorporates some

of the experimental data available for the actual width of the bands (see Figure 6 for HQ).

Although the optical spectra simulated by the present study are generally similar to those obtained by BGC, the maxima are shifted slightly toward lower wavelengths and once again probably reflect the occasional differences that arise in the structural geometries and the different CI schemes used by the two approaches.

Dimers. Among the five dimer configurations examined, the entirely planar structure (Figure 7c) was found to have the lowest energy and, therefore, to be the most stable, as predicted by both the LDA and GGA functionals. Physically, this result is in accord with the stabilization afforded by the hydrogen bond that is formed between the hydrogen associated with the indole moiety and the adjacent carbonyl.

Dimer 3, the dimer of interest to us here, shows a strong bathochromic shift in absorption (toward longer wavelengths). We believe that this is because the relatively planar structure associated with this particular dimer corresponds to more extensive delocalization, which, in turn, produces lower-energy transitions. The lowest-energy transition expected for the structure of the dimer in Figure 7c is illustrated in Table 6, where the HOMO−LUMO energy gaps are listed. This feature is expected to play an important role in explaining the absorption spectrum of the full oligomer, melanin structure. Correlations between HOMO−LUMO gaps and torsion angles across the dimer bond as well as the maximum absorption wavelength have been found.

Another correspondence between the results of the present simulations and experimental results for melanin relates to the issue of planarity that is predicted for the dimers and higher oligomers. This important structural feature corresponds well with the successful X-ray diffraction modeling of experimental data derived from melanin powders that best fit the X-ray data with planar oligomeric structures.

The results of this work indicate sufficient agreement with the work of BGC and sufficient correspondence with published experimental work to warrant an extension of the methodology to include the higher oligomeric units believed to represent the molecular structure of eumelanins.

References and Notes

(1) Prota, G. *Melanins and Melanogenesis*; Academic Press: New York, 1992.

(2) Ziese, L., Chedekel, M. R., Fitzpatrick, T. B., Eds. *Melanin: Its Role in Human Protection*; American Society for Photobiology: Lawrence, KS, 1995.

(3) Swan, G. A. *Ann. N.Y. Acad Sci*. **1963**, *100*, 1005.

(4) Swan, G. A. *Fortschr. Chem. Org. Naturst.* **1974**, *31*, 522.

(5) Chio, S. S. X-ray Diffraction and ERS Studies on Amorphous Melanin. Ph.D. Thesis, University of Houston, Houston, TX, 1977.

(6) D′Ischia, M.; Napolitano, A.; Prota, G. *Gazz. Chim. Ital*. **1996**, *126*, 783.

(7) Cheng, J.; Moss, S. C.; Eisner, M.; Zschack, P. *Pigm. Cell Res*. **1994**, *7*, 255−262.

(8) Cheng, J.; Moss, S. C.; Eisner, M. *Pigm. Cell Res.* **1994**, 7, 263−273.

(9) Zajac, G. W.; Gallas, J. M.; Cheng, J.; Eisner, M.; Moss, S. C.; Alvarado-Swaisgood, A. E. *Biochim. Biophys. Acta* **1994**, *1199*, 271.

(10) Gallas, J. M.; Zajac, G. W.; Sarna, T.; Stotter, P. L. *Pigm. Cell Res.* **2000**, *13*, 99.

(11) Zajac, G. W.; Gallas, J. M.; Alvarado-Swaisgood, A. E. *J. Vacuum Sci. Technol. B* **1994**, *12*, 1512.

(12) Simon, J. D. *Acc. Chem. Res.* **2000**, *33*, 307.

(13) Gallas, J. M.; Littrell, K. C.; Seifert, S.; Zajac, G. W.; Thiyagarajan, P. *Biophys. J.* **1999**, *77*, 1135.

(14) Clancy, C. M. R.; Simon, J. D. *Biochemistry* **2001**, *40*, 13353.

(15) Bolivar-Marinez, L. E.; Galvao, D. S.; Caldas, M. J. *J. Phys. Chem. B* **1999**, *103*, 2993.

(16) Miyake, Y.; Izumi, Y.; Tsutsumi, A.; Jimbow, K. Chemico-physical properties of melanin III. In *Structure and Function of Melanin 3*; Jimbow, K., Ed.; Fuji Ltd.: Sappora, Japan, 1986; pp 3−18.

(17) Galvao, D. S.; Caldas, M. J. *J. Chem Phys*. **1988**, *88*, 4088.

(18) Galvao, D. S.; Caldas, M. J. *J. Chem. Phys*. **1990**, *92*, 2630.

(19) Galvao, D. S.; Caldas, M. J. *J. Chem. Phys*. **1990**, *93*, 2848.

(20) Delley, B. *J. Chem. Phys.* **1990**, *92*, 508; *J. Chem. Phys.* **2000**, *113*, 7756. $DMol^3$ is available as part of Materials Studio by Accelrys Inc.

(21) Delley, B. In *Density Functional Theory: A Tool for Chemistry*; Seminario, J. M., Politzer, P., Eds.; Elsevier: Amsterdam, The Netherlands, 1995.

(22) Vosko, S. J.; Wilk, L.; Nusair, M. *Can. J. Phys*. **1980**, *58*, 1200.

(23) Becke, A. D. *J. Chem. Phys.* **1988**, *88*, 2547. Perdew, J. P. In *Electronic Structure of Solids*; Ziesche, P., Eschrig, H., Eds.; Akademie Verlag: Berlin, 1991; p 11. Perdew, J. P.; Wang, Y. *Phys. Rev. B* **1992**, *45*, 13244.

(24) Materials Studio $DMol^3$ version 2.1.

(25) Pulay, P.; Fogarasi, G.; Pang, F.; Boggs, J. E. *J. Am. Chem. Soc*. **1979**, *101*, 2550. Baker, J.; Kessi, A.; Delley, B. *J. Chem. Phys.* **1996**, *105*, 192. Andzelm, J.; King-Smith, R. D.; Fitzgerald, G. *Chem. Phys. Lett.* **2001**, *335*, 321.

(26) Clark, T.; Chandrasekhar, J. *Israel J. Chem*. **1993**, *33*, 435. Clark T. In *Recent Experimental and Computational Advances in Molecular Spectroscopy*; NATO ASI Series C; Fausto, R. Ed.; Kluwer Academic Publishers: Dordrecht, The Netherlands, 1993; Vol. 406, p 369.

(27) Dewar, M. J. S.; Zoebisch, E. G.; Healy, E. F.; Stewart, J. J. P. *J. Am. Chem. Soc.* **1985**, *107*, 3902.

(28) Clark, T.; Alex, A. Beck, B.; Burkhardt, F.; Chandrasekhar, J.; Gedeck, P.; Horn, A.; Hutter, M.; Martin, B.; Rauhut, G.; Sauer, W.; Schindler, T.; Steinke, T. *VAMP*, version 8.0; Universität Erlangen, Erlangen, Germany, 2001. This version is provided as part of Materials Studio 2.1 by Accelrys Inc.

(29) Andzelm, J.; Wimmer, E. *J. Chem. Phys*. **1992**, *96*, 1280.

(30) (a) Painter, G. S.; Averill, F. W. *Phys. Rev. B* **1982**, *26*, 1781. Jones, R. O. *J. Chem. Phys.* **1982**, *76*, 3098. (b) Johnson, B. G.; Gill, P. M. W.; Pople, J. A. *J. Chem. Phys*. **1993**, *98*, 5612.

(31) Dickson, R. M.; Becke, A. D. *J. Phys. Chem*. **1993**, *99*, 3898.

(32) Amos, R. D.; Murray, C. W.; Handy, N. C. *Chem. Phys. Lett*. **1993**, *202*, 489.

(33) Altman, J. A.; Handy, N. C.; Ingamells, V. E. *Int. J. Quantum Chem.* **1996**, *57*, 533.

(34) Scheiner, A. C.; Baker, J.; Andzelm, J. *J. Comput. Chem*. **1997**, *18*, 775.

(35) Stewart, J. J. P. *J. Comput. Chem*. **1989**, *10*, 209.

(36) Ridley, J.; Zerner, M. *Theor. Chem. Acta* **1987**, *42*, 347.

(37) Dos Santos, D. A.; Galvao, D. S.; Lake, B.; Dos Santos, M. C. *Chem. Phys. Lett.* **1991**, *184*, 579 and references therein.

(38) Parusel, A. J. B. Paper included in Photobiology 99 (Second Internet Conference on Photochemistry and Photobiology), Jul 16−Sep 7, 1999 (available at http://www.photobiology.com/photobiology99/contrib/parusel/index.htm).

(39) Maheshwari, S.; Chowdhury, A; Sathyamurthy, S.; Mishra, H.; Tripathi, H. B.; Panda, M.; Chandrasekhar, J. *J. Phys. Chem. A* **1999**, *103*, 6257.

(40) Ziegler, T.; Li, J. *Can. J. Chem*. **1994**, *72*, 743.

(41) Wimmer, E. *Computational Methods for Atomistic Simulations of Materials*; Accelrys: San Diego, CA (available at http://www.accelrys.com/technology/qm/erich/).